ISSN: 2164-0165 Vol. 5, No. 1, February 2015

Scientific Research Publishing

Modern Mechanical Engineering

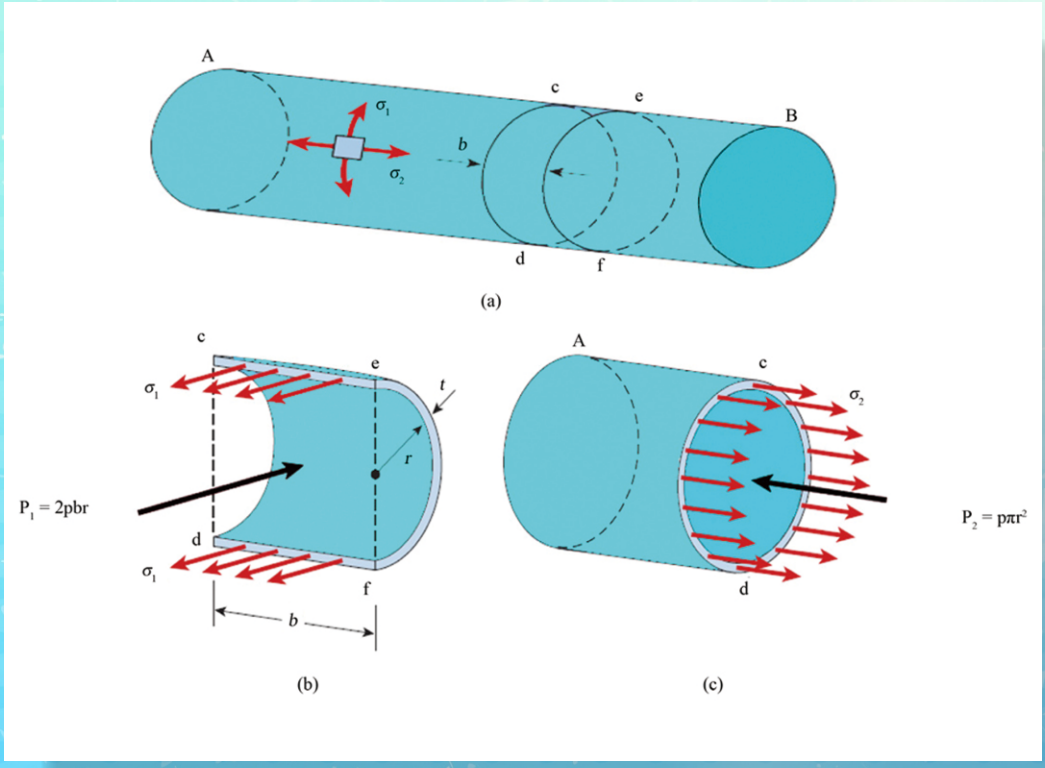

ISSN: 2164-0165

www.scirp.org/journal/mme

Journal Editorial Board

ISSN Print: 2164-0165 ISSN Online: 2164-0181
http://www.scirp.org/journal/mme

Editor in Chief

Editorial Board

Modern Mechanical Engineering, 2015, 5, 1-19
Published Online February 2015 in SciRes. http://www.scirp.org/journal/mme

Table of Contents

Volume 5 Number 1 February 2015

The figure on the front cover is from the article published in Modern Mechanical Engineering, 2015, Vol. 5, No. 1, pp. 1-9 by Ahmed Ibrahim, Yeong Ryu and Mir Saidpour.

Modern Mechanical Engineering (MME)

Journal Information

SUBSCRIPTIONS

The *Modern Mechanical Engineering* (Online at Scientific Research Publishing, www.SciRP.org) is published quarterly by Scientific Research Publishing, Inc., USA.

Subscription rates:

Print: $69 per issue.
To subscribe, please contact Journals Subscriptions Department, E-mail: sub@scirp.org

SERVICES

Advertisements
Advertisement Sales Department, E-mail: service@scirp.org

Reprints (minimum quantity 100 copies)
Reprints Co-ordinator, Scientific Research Publishing, Inc., USA.
E-mail: sub@scirp.org

COPYRIGHT

PRODUCTION INFORMATION

For manuscripts that have been accepted for publication, please contact:
E-mail: mme@scirp.org

Modern Mechanical Engineering, 2015, 5, 1-9
Published Online February 2015 in SciRes. http://www.scirp.org/journal/mme
http://dx.doi.org/10.4236/mme.2015.51001

Stress Analysis of Thin-Walled Pressure Vessels

Ahmed Ibrahim*, Yeong Ryu, Mir Saidpour

Mechanical Engineering Technology, Farmingdale State College, Farmingdale, New York, USA
Email: *ahmed.ibrahim@farmingdale.edu, yeong.ryu@farmingdale.edu, mir.saidpour@farmingdale.edu

Received 15 January 2015; accepted 1 February 2015; published 3 February 2015

Abstract

This paper discusses the stresses developed in a thin-walled pressure vessels. Pressure vessels (cylindrical or spherical) are designed to hold gases or liquids at a pressure substantially higher than the ambient pressure. Equations of static equilibrium along with the free body diagrams will be used to determine the normal stresses σ_1 in the circumferential or hoop direction and σ_2 in the longitudinal or axial direction. A case study of internal pressure developed in a soda can was determined by measuring the elastic strains of the surface of the soda can through strain gages attached to the can and connected to Strain indicator Vishay model 3800.

Keywords

Stress Analysis, Thin-Walled Pressure Vessel

1. Introduction

Pressure vessels are compressed gas storage tanks designed to hold gases or liquids at a pressure substantially different from the ambient pressure. They have a variety of applications in industry, including in oil refineries, nuclear reactors, gas reservoirs, etc. An aircraft fuselage, a gas cylinder and a soda can, all are pressure vessels which must be designed to meet very specific requirements of integrity. The human arteries maintain pressure in the circulatory system much like a balloon maintains pressure on the air within it. The arteries therefore act as pressure vessels by maintaining pressure. Pressure vessels can be any shape, but shapes made of sections of spheres and cylinders are usually employed. A common design is a cylinder with end caps called heads. Head shapes are frequently hemispherical.

Cracked or damaged vessels can result in leakage or rupture failures. Potential health and safety hazards of leaking vessels include poisonings, suffocations, fires, and explosion hazards. Rupture failures can be much

*Corresponding author.

How to cite this paper: Ibrahim, A., Ryu, Y. and Saidpour, M. (2015) Stress Analysis of Thin-Walled Pressure Vessels. *Modern Mechanical Engineering*, **5**, 1-9. http://dx.doi.org/10.4236/mme.2015.51001

more catastrophic and can cause considerable damage to life and property. The safe design, installation, operation, and maintenance of pressure vessels are in accordance with codes such as American Society of Mechanical Engineers (ASME) boiler and pressure vessel code [1]. Therefore, great emphasis should be placed on analytical and experimental methods for determining their operating stresses.

Spherical Pressure Vessel, like the one shown in **Figure 1**, is preferred for storage of high pressure fluids. A spherical pressure vessel has approximately twice the strength of a cylindrical pressure vessel with the same wall thickness. A sphere is a very strong structure. The distribution of stresses on the sphere's surfaces, both internally and externally are equal. Spheres however, are much more costly to manufacture than cylindrical vessels. A spherical storage has a smaller surface area per unit volume than any other shape of vessel. This means, that the quantity of heat transferred from warmer surroundings to the liquid in the sphere, will be less than that for cylindrical storage vessels.

Pressure vessels are subjected to tensile forces within the walls of the container. The normal stress in the walls of the container is proportional to the pressure and radius of the vessel and inversely proportional to the thickness of the walls [2] [3]. As a general rule, pressure vessels are considered to be thin-walled when the ratio of radius r to wall thickness t is greater than 10 [4]. Pressure vessels fail when the stress state in the wall exceeds some failure criterion [5] [6]. Therefore pressure vessels are designed to have a thickness proportional to the radius of tank and the pressure of the tank and inversely proportional to the maximum allowed normal stress of the particular material used in the walls of the container. Thus, it is important to understand and quantify (analyze) stresses in pressure vessels. In this paper we will analyze the stresses in thin-walled pressure vessels (cylindrical & spherical shapes), like the one shown in **Figure 1** & **Figure 2**. In addition, a case study of internal stresses developed in a soda can will be presented and discussed.

Figure 1. Japanese gas companies added a touch of character to giant spherical gas tanks.

Figure 2. Cylindrical pressure vessel in a chemical plant.

2. Thin-Walled-Cylindrical Pressure Vessel

A thin-walled circular tank AB subjected to internal pressure shown in **Figure 3**. A stress element with its faces parallel and perpendicular to the axis of the tank is shown on the wall of the tank. The normal stresses σ_1 and σ_2 acting on the side faces of this element. No shear stresses act on these faces because of the symmetry of the vessel and its loading. Therefore, the stresses σ_1 and σ_2 are principal stresses. Because of their directions, the stress σ_1 is called the circumferential stress or the hoop stress, and the stress σ_2 is called the longitudinal stress or the axial stress. Each of these stresses can be calculated from static equilibrium equations.

Several assumptions have been made to derive the following equations for circumferential and longitudinal stresses:

1) Plane sections remain plane
2) $r/t \geq 10$ with t being uniform and constant
3) Material is linear-elastic, isotropic and homogeneous.
4) Stress distributions throughout the wall thickness will not vary
5) Weight of the fluid is considered negligible.

3. Circumferential Stress

To determine the circumferential stress σ_1, make three sections (cd and ef) perpendicular to the longitudinal axis and distance b apart (**Figure 3(a)**); and a third cut in a vertical plane through the longitudinal axis of the tank. The resulting free body diagram is shown in **Figure 3(b)**. Acting on the longitudinal cut (plane cefd) are the circumferential stresses σ_1 and the internal pressure p.

The circumferential stresses σ_1 acting in the wall of the vessel have a resultant equal to $\sigma_1(2bt)$, where t is the thickness of the wall. Also, the resultant force P_1 of the internal pressure is equal to $2pbr$, where r is the inner radius of the cylinder. Hence, we have the following equation of equilibrium:

$$\sigma_1(2\text{bt}) - 2\text{pbr} = 0$$

From the above equation, the circumferential stress in a pressurized cylinder can be found:

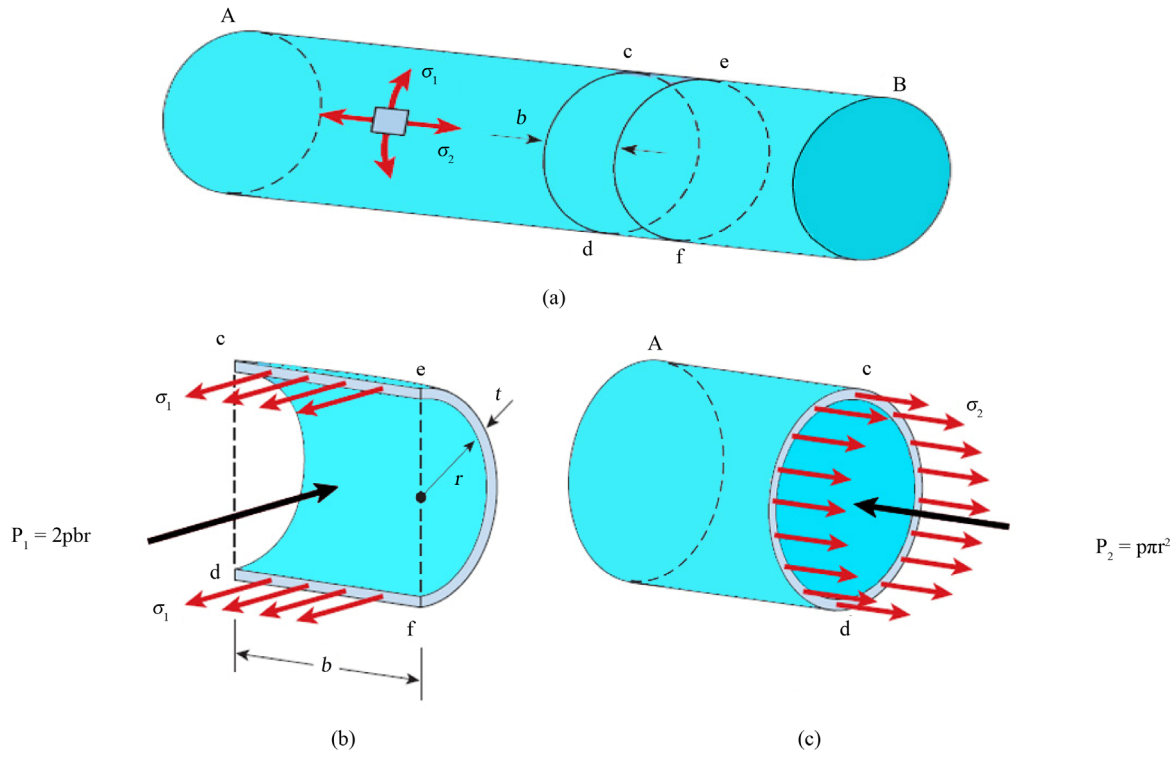

Figure 3. Stresses in a circular cylindrical presure vessel.

$$\sigma_1 = \frac{pr}{t} \tag{1}$$

If there exist an external pressure p_o and an internal pressure p_i, the formula may be expressed as:

$$\sigma_1 = \frac{(p_i - p_o)r}{t} \tag{2}$$

4. Longitudinal Stress

The longitudinal stress σ_2 is obtained from the equilibrium of a free body diagram shown in **Figure 3(c)**. The stresses σ_2 acts longitudinally and have a resultant force equal to σ_2 $(2\pi rt)$. The resultant force P_2 of the internal pressure is a force equal to $p\pi r^2$. The equation of equilibrium for the free body diagram is

$$\sigma_2(2\pi rt) - p\pi r^2 = 0$$

Solving the above equation for σ_2, lead to the following formula for the longitudinal stress in a cylindrical pressure vessel:

$$\sigma_2 = \frac{pr}{2t} \tag{3}$$

If there exist an external pressure p_o and an internal pressure p_i, the formula may be expressed as:

$$\sigma_1 = \frac{(p_i - p_o)r}{2t} \tag{4}$$

Comparing Equations (1) and (3) we find that the circumferential stress in a cylindrical vessel is equal to twice the longitudinal stress:

$$\sigma_1 = 2\sigma_2 \tag{5}$$

Due to this, cylindrical pressure vessels will split on the wall instead of being pulled apart like it would under an axial load.

5. Stresses at the Outer Surface

The principal stresses σ_1 and σ_2 at the outer surface of a cylindrical vessel are shown on the stress element of **Figure 4(a)**. The element is in biaxial stress (stress in *z* direction is zero).

The maximum in-plane shear stresses occur on planes that are rotated 45˚ about the *z* axis:

$$(\tau_{\max})_z = \frac{(\sigma_1 - \sigma_2)}{2t} = \frac{\sigma_1}{4} = \frac{pr}{4t}$$

The maximum out-of-plane shear stresses occur on planes that are rotated 45˚ about x and y axes, respectively:

$$(\tau_{\max})_x = \frac{\sigma_1}{2} = \frac{pr}{2t}$$

$$(\tau_{\max})_y = \frac{\sigma_2}{2} = \frac{pr}{4t}$$

Therefore, the maximum absolute shear stress is:

$$\tau_{\max} = \frac{\sigma_1}{2} = \frac{pr}{2t} \tag{6}$$

Occurs on a plane rotated by 45˚ about the *x*-axis.

6. Stresses at the Inner Surface

The stress conditions at the inner surface of the wall of the vessel are shown in **Figure 4(b)**. The principal stresses

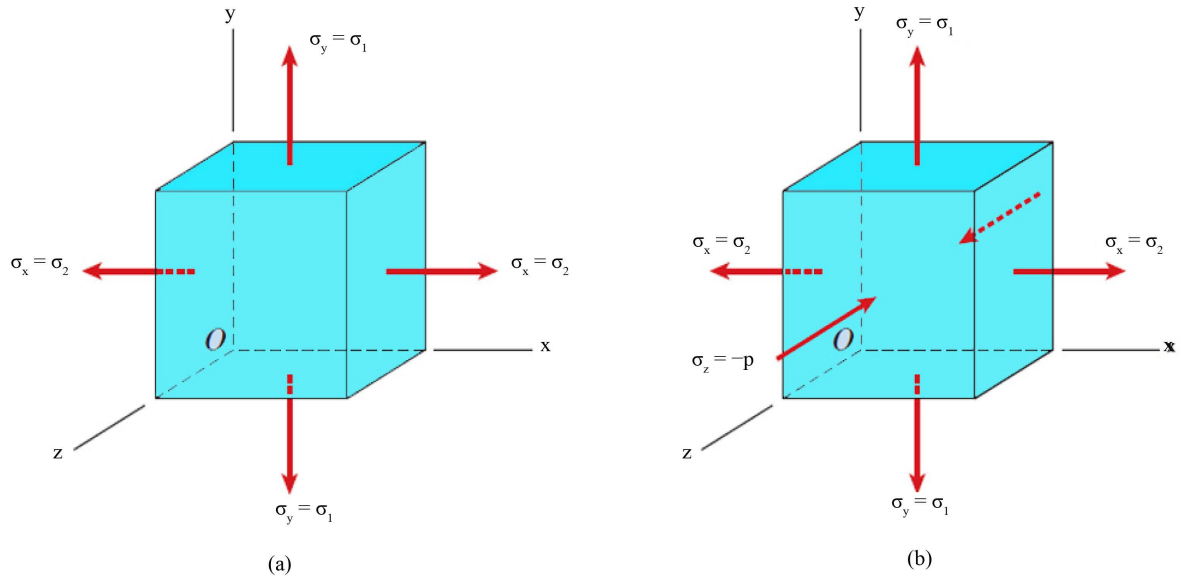

Figure 4. Stresses in a circular cylindrical pressure vessel at (a) the outer surface, (b) the inner surface.

are:

$$\sigma_1 = \frac{pr}{t}, \quad \sigma_2 = \frac{pr}{2t}, \quad \sigma_3 = -p$$

The three maximum shear stresses, obtained by 45˚ rotations about the x, y, and z axes, are

$$(\tau_{\max})_x = \frac{(\sigma_1 - \sigma_3)}{2} = \frac{pr}{2t} + \frac{p}{2} \tag{7}$$

$$(\tau_{\max})_y = \frac{(\sigma_2 - \sigma_3)}{2} = \frac{pr}{4t} + \frac{p}{2} \tag{8}$$

$$(\tau_{\max})_z = \frac{(\sigma_1 - \sigma_2)}{2} = \frac{pr}{4t} \tag{9}$$

When r/t is very large (thin walled), the term $p/2$ can be disregarded, and the equations are the same as the stresses at the outer.

7. Spherical Pressure Vessel

A similar approach can be used to derive an expression for an internally pressurized thin-wall spherical vessel. A spherical pressure vessel is just a special case of a cylindrical vessel.

To find σ we cut the sphere into two hemispheres as shown in **Figure 5**. The free-body diagram gives the equilibrium condition $\sigma 2\pi rt = p\pi r^2$, hence

$$\sigma = \sigma_h = \sigma_a = \frac{pr}{2t} \tag{10}$$

Any section that passes through the center of the sphere yields the same result. Comparing Equations (1), (3), and (10) yields that for the same p, r and t the spherical geometry is twice as efficient in terms of wall stress.

As shown in **Figure 6**, the internal pressure of the cylindrical vessel is resisted by the hoop stress in "arch action" whereas the axial stress does not contribute. In the spherical vessel the double curvature means that all stress directions around the pressure point contribute to resisting the pressure.

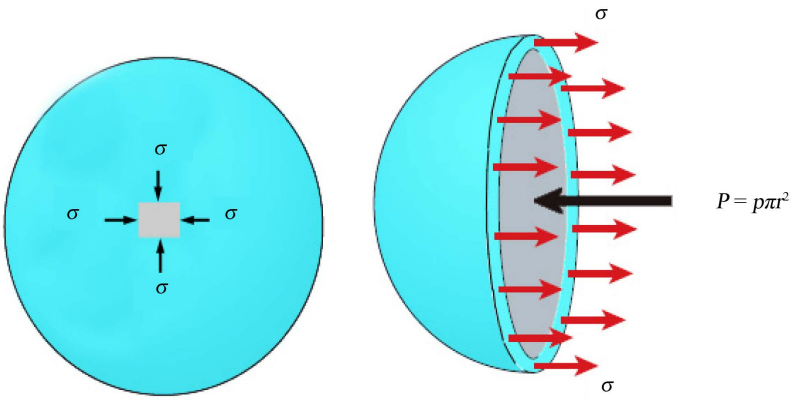

Figure 5. Stresses in a spherical pressure vessel.

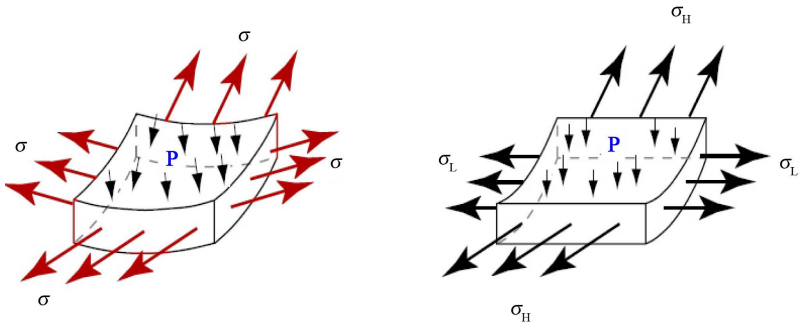

Figure 6. (a) Spherical pressure vessel; (b) Cylindrical pressure vessel.

8. Case Study: Measuring Internal Pressure in a Soda Can Using Strain Gauges

The soda can is analyzed as a thin wall pressure vessel. In a thin wall pressure vessel, two stresses exist: the longitudinal stress (σ_L) and the hoop stress (σ_H) (**Figure 7**). The longitudinal stress is a result of the internal pressure acting on the ends of the cylinder and stretching the length of the cylinder as shown in **Figure 8**. The hoop stress is the result of the radial action of the internal pressure that tends to increase the circumference of the can.

The pressure developed in a soda can be determined by measuring the elastic strains of the surface of the soda can. Internal pressure for a pressurized soda can be derived using basic Hooke's law stress and strain relations that relate change in hoop and axial strains to internal pressure. Two strain gauges (Measurements Group-CEA series gages) was attached to the soda can (**Figure 9**) to measure the change in strains, as measured through the voltage across a calibrated Wheatstone bridge. M-bond 200 adhesive (Measurements Group, Inc) was used to glue the strain gages to the surface of the soda can.

The hoop stress for the thin walled cylinder can be calculated from Equation (1)

$\sigma_H = \dfrac{pr}{t}$ where:

p—internal pressure (psi)
D—mean diameter of cylinder (in.)
t—wall thickness (in.)
Similarly, the longitudinal stress cylinder wall can be calculated from Equation (3)

$$\sigma_L = \frac{pr}{2t}$$

Equation (5) yields

$$\sigma_H = 2\sigma_L$$

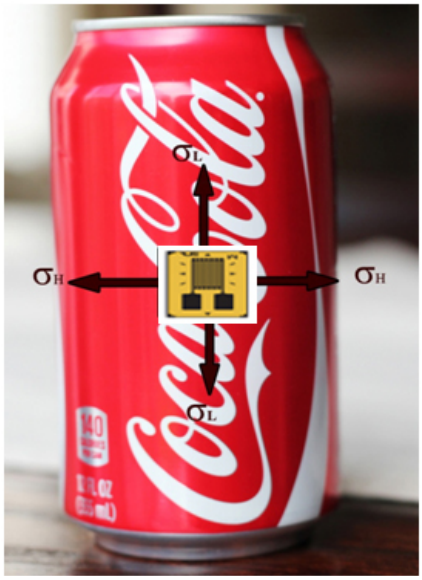

Figure 7. Coca cola soda can.

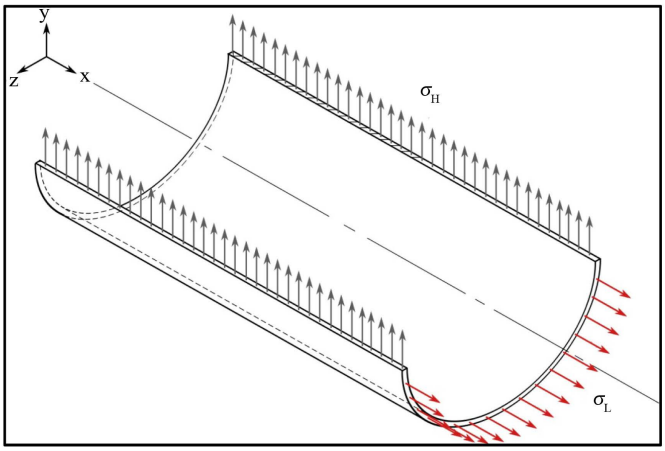

Figure 8. Longitudinal stress distribution.

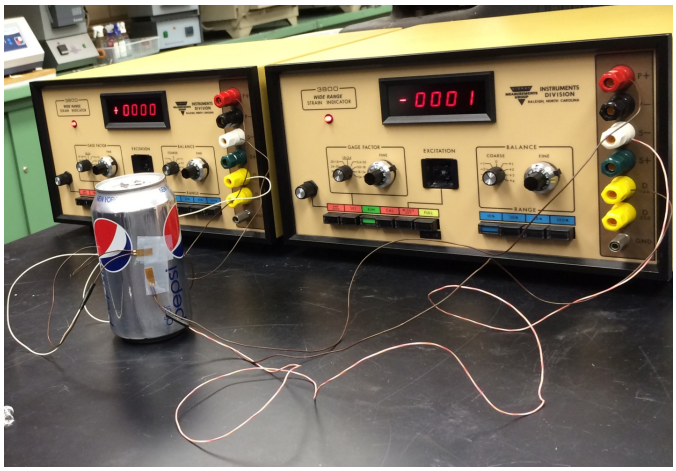

Figure 9. Strain gages attached to a soda can and strain indicator vishay model 3800.

Assuming that:

- The material is homogeneous and isotropic,
- The can is loaded only within its elastic range,
- A biaxial state of stress exists in the can,

The internal stresses developed in the soda can are proportional to the elastic strains of the outside surface of the soda can as follow:

$$\sigma_L = \frac{E\left(\varepsilon_L - \nu\varepsilon_H\right)}{\left(1-\nu^2\right)} \tag{11}$$

$$\sigma_H = \frac{E\left(\varepsilon_H - \nu\varepsilon_L\right)}{\left(1-\nu^2\right)} \tag{12}$$

where:

E —modulus of elasticity or Young's modulus (psi)

ν —Poisson's ratio

ε_H —hoop strain (in/in)

ε_L —longitudinal strain (in/in)

Using Equations (11) and (12) with Equation (5), and simplifying results in:

$$\sigma_L = \frac{E\varepsilon_H}{\left(2-\nu\right)} \tag{13}$$

$$\sigma_H = \frac{E\varepsilon_L}{\left(1-2\nu\right)} \tag{14}$$

Thus the pressure can be calculated directly from the measured strains by substituting Equations (13) and (14) back into Equation (1) and (2) to get:

$$p = \frac{4tE\varepsilon_H}{D\left(2-\nu\right)} \tag{15}$$

$$p = \frac{4tE\varepsilon_L}{D\left(1-2\nu\right)} \tag{16}$$

Once we have Equations (15) and (16), then the internal pressure in the can may be directly calculated from the measured longitudinal and hoop strains.

9. Internal Pressure Results

Measured Values

Can thickness: t = 0.004 in

Can diameter: D = 2.59 in

Young's Modulus: E = 10 × 106 psi (assumed)

Poisson's Ratio: ν = 0.3

The change in longitudinal and hoop strains were measured after the pressure was released from the cans. The results of the strains and corresponding pressures are shown in **Table 1**.

10. Conclusion

This paper presented a detailed stress analysis of the stresses developed in thin-walled pressure vessels (cylindrical & spherical). Then, a case study of a soda can that was analyzed as a thin wall pressure vessel was discussed. The elastic strains (ε_H & ε_L) of the external surface of the soda can was determined through strain gages attached to the can surface and connected to a strain indicator. The longitudinal stress, hoop stress, and the internal pressure were determined from equations of generalized Hooke's law for stress and strain. Small varia-

Table 1. Elastic strains and corresponding internal pressures in a Soda can.

Test		Strain × 10^{-6} in/in	Internal Pressure (psi)
1	Longitudinal	−275	−42.5
	Hoop	−1248	−45.4
2	Longitudinal	−295	−45.6
	Hoop	−1172	−42.2
3	Longitudinal	−224	−41.3
	Hoop	−1156	−42

tions recorded in internal pressures calculated from the longitudinal strain (ε_L) and the hoop strain (ε_H).

References

[1] Rao, K. (2012) Companion Guide to the ASME Boiler and Pressure Vessel Code, Volume 1, Fourth Edition, ASME. http://dx.doi.org/10.1115/1.859865

[2] Gere, J. and Timoshenko, S. (1997) Mechanics of Materials. 4th Edition, PWS, 549. http://dx.doi.org/10.1007/978-1-4899-3124-5

[3] Moss, D. (2013) Pressure Vessel Design Manual. Elsevier. http://dx.doi.org/10.1016/b978-0-12-387000-1.10032-4

[4] Freyer, D. and Harvey, J. (1998) High Pressure Vessels. Springer, Berlin, 11. http://dx.doi.org/10.1007/978-1-4615-5989-4

[5] Annaratone, D. (2007) Pressure Vessel Design. Springer, Berlin, 47-125. http://dx.doi.org/10.1007/978-3-540-49144-6

[6] Shigley, J. (1983) Mechanical Engineering Design. 4th Edition, McGraw-Hill, New York, 70. http://dx.doi.org/10.1115/1.3258702

Modern Mechanical Engineering, 2015, 5, 10-19
Published Online February 2015 in SciRes. http://www.scirp.org/journal/mme
http://dx.doi.org/10.4236/mme.2015.51002

An ARX-Based PID-Sliding Mode Control on Velocity Tracking Control of a Stick-Slip Piezoelectric-Driven Actuator

Y. Cao, X. B. Chen

Department of Mechanical Engineering, University of Saskatchewan, Saskatoon, Canada
Email: yuc150@mail.usask.ca

Received 20 January 2015; accepted 8 February 2015; published 11 February 2015

Abstract

Piezoelectric-driven stick slip actuators have been drawn more and more attention in the nano-positioning application due to the high accuracy and theoretical unlimited displacement. However, the hysteresis of piezoelectric actuator (PEA) and the nonlinear friction force between the end-effector and the stage make control of piezoelectric-driven stick slip actuator challenge. This paper presents the development of an autoregressive exogenous (ARX)-based proportional-integral-derive (PID)-sliding mode control (SMC) for the velocity tracking control of the piezoelectric-driven stick slip actuator. Stability is guaranteed by rigorously choosing the appropriate PID parameters and the zero steady state error is achieved. To verify the effectiveness of the proposed method, experiments were carried out on a commercially-available piezoelectric-driven stick slip actuator. The tracking errors were compared with the traditional PID controller, illustrating that in spite of existing of modeling error, the ARX-based PID-SMC is able to better improve the velocity tracking performance of piezoelectric-driven stick slip actuator, compared with the traditional PID controller.

Keywords

Autoregresive Progress, Sliding Mode Control, Slick-Slip, Piezoelectric Actuator

1. Introduction

Piezoelectric-driven stick-slip actuators play important roles in nano-positioning applications due to their simple configuration, high accuracy and theoretically unlimited displacement [1]-[6]. The end-effector is supported and guided by a movable stage, which is connected to the base through flexible hinges and driven by a PEA, as

How to cite this paper: Cao, Y. and Chen, X.B. (2015) An ARX-Based PID-Sliding Mode Control on Velocity Tracking Control of a Stick-Slip Piezoelectric-Driven Actuator. *Modern Mechanical Engineering*, **5**, 10-19.
http://dx.doi.org/10.4236/mme.2015.51002

shown in **Figure 1**. The end-effector moves together with the stage under slow expansion of the PEA. Sudden contraction of the PEA leads to the sliding motion of the end-effector since the force due to the friction limit between the end-effector and the movable stage. As a result, the end-effector moves a step ΔS, with respect to its original position. Such steps can be accumulated to achieve a theoretically unlimited displacement (actually limited by the size of the moveable stage).

The hysteresis of PEA and the friction dynamics of the end-effector make the control of stick-slip actuator challenge. An analog electronic circuit was developed in [7] for driving stick-slip piezoelectric linear actuators. The key design task for the amplifier is to provide a high-voltage asymmetric sawtooth-like signal and feed it into a capacitive load. To compensate the hysteresis effect, combination of a charge control scheme with switching is proposed and the experiments confirm the superiority of the proposed method over other existing techniques. However, the charge control requires expensive hardware, which increases the difficulty and cost of its implementation. To avoid this, a voltage/frequency proportional controller was proposed in [8] for high stroke displacement of stick-slip micro-positioning stage. The proposed controller is essentially a combination of the sign controller, the classical proportional control and frequency proportional control, and the experimental results showed its priority over the basic controller. To compensate the steady state error, integral control was employed in addition to the aforementioned method [9]. In [10], Proportional-Derivative (PD) controller was applied in the control of the stick slip piezoelectric actuators. Its application in the sample holder for Atomic Force Microscope (AFM), the micro-Electrical Discharge Machining (EDM) machine, the micro-assembly system and the micro tele-manipulation system for biological specimens was described.

All the research mentioned above related to the displacement tracking control of the piezoelectric-driven stick-slip actuators under step or ramp reference signal. The velocity tracking control has not been reported yet. This work focuses on the development of control method for the velocity tracking control of the piezoelectric-driven stick-slip actuators.

PID/PI/PD controller has shown great potential in the control application for nano-positioners. The challenge of PID/PI/PD control in the velocity tracking control of stick-slip piezoelectric-driven stage is maintaining the system stability in the presence of uncertainty and disturbance. It also has an issue with low gain margin in high frequency applications [1]. Recently, sliding model control (SMC) has been drawing considerable attention in the control research community worldwide due to its ability to compensate for the system uncertainties and disturbance [11]-[14]. To solve the chattering problem of the regular SMC, a PID-based SMC (PID-SMC) was developed in [15], in which the discontinuous “bang-bang” switching function is replaced by a PID regulator. Due to the integral effect of the PID regulator, zero steady state tracking error can be achieved.

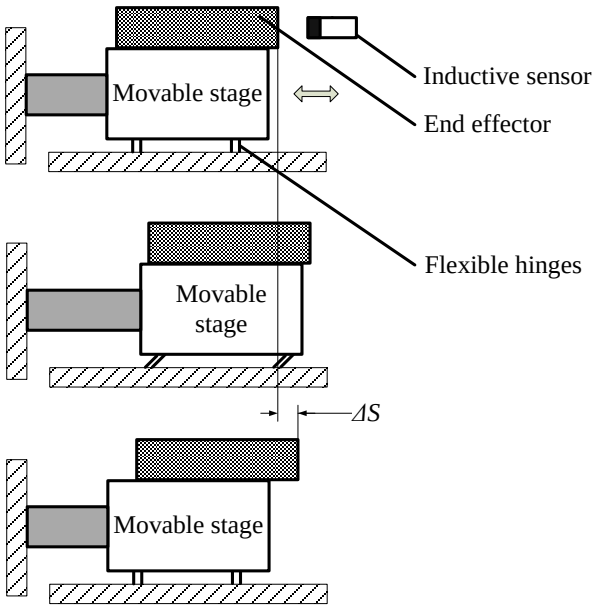

Figure 1. Working principle of the piezoelectric-driven stick-slip actuator.

As a state tracking control scheme, the PID-SMC developed in [15] has been shown effective in the control of the second order mechanical systems, in which the states can be readily estimated from the measured output and/or its derivatives. In some circumstances, the system state might not be readily or even be impossibly obtained due to system complexity. In such a case, the application of PID-SMC is challenged due to the lack of system state information. For this, an output tracking integrated PID-SMC is developed [16], in which the transfer function of the plant is considered to be a cascade of the numerator and the denominator. The numerator is compensated by an optimal inverse feedforward controller and as such the regular state tracking based SMC can be applied. The proposed method has been experimentally shown effective in the control of a commercially available one-degrees-of-freedom (DOF) piezoelectric actuator.

It is noted that if the dynamics of the plant can be represented by an auto-regressive (ARX) model without zeros, for example, $y(k)=\sum_{i=1}^{n} a_i y(k-i)+bu(k-1)$, where $u(k)$ and $y(k)$ are the system input and output at time instant k respectively, such a model will be readily transferred to a state space model with its state being the system output and the state tracking based PID-SMC is able to be directly applied for the dynamics compensation. Inspired by this, an ARX-based PID-SMC is developed in this paper and applied in the velocity control of a one-DOF stick-slip PEA. The effectiveness of the proposed method is experimentally verified and compared with the traditional PID controller introduced in [9].

2. ARX-Based PID-SMC and Its Design

The discrete nth order plant might be generally described by the following transfer function

$$G(z)=\frac{\sum_{j=0}^{n}\beta_i z^{-j}}{1+\sum_{i=1}^{n}\alpha_i z^{-i}}. \tag{1}$$

where $\alpha_i, \beta_i\ (i=1,2,\cdots,n)$ and β_0 are the parameters and the numerator and denominator are relatively prime polynomials. With the use of the system identification method, this plant model can be mathematically represented by an ARX model.

$$y(k)=\sum_{i=1}^{n} a_i y(k-i)+bu(k-1)+\varepsilon(k-1). \tag{2}$$

Equation (2) is identical to a discrete transfer function without zeros. The neglect of zeros definitely leads to model errors, which is considered to be disturbance in Equation (2).

The ARX model can be rewritten in a state space form

$$x(k+1)=Ax(k)+Bu(k)+D\varepsilon(k). \tag{3}$$

where $x(k)=\begin{bmatrix} y(k-n) & \cdots & y(k-2) & y(k-1)\end{bmatrix}^{\mathrm{T}}\in R^{n\times 1}$ is the state vector; $A=\begin{bmatrix} 0_{(n-1)\times 1} & I_{(n-1)\times(n-1)} \\ -a_n & \boldsymbol{a}\end{bmatrix}$ $\left(\boldsymbol{a}=\begin{bmatrix}-a_{n-1} & -a_{n-2} & \cdots & -a_1\end{bmatrix}\right)$, $B=\begin{bmatrix}0_{1\times(n-1)} & \beta_0\end{bmatrix}^{\mathrm{T}}$ and $D=\begin{bmatrix}0_{1\times(n-1)} & 1\end{bmatrix}^{\mathrm{T}}$ are the system matrixes of the discrete state space model. The state vector is represented in terms of the outputs in the past history, which suggest the state tracking is essentially the output tracking. Therefore, the state tracking SMC design method can be applied.

Denote the desired output vector to be $x_d(k)=\begin{bmatrix} y_d(k-n) & \cdots & y_d(k-2) & y_d(k-1)\end{bmatrix}^{\mathrm{T}}\in R^{n\times 1}$. The objective of SMC is to force the error state $e(k)=x(k)-x_d(k)$ to move to the sliding surface and then converge to zero. Equation (3) can be rewritten in terms of the dynamics of $e(k)$,

$$e(k+1)=Ae(k)+Bv(k)+D\varepsilon(k)+Ax_d(k)-x_d(k+1). \tag{4}$$

Similar to the general SMC design approach introduced in [15], the input $u(k)$ is divided into two parts $u_1(k)$ and $u_{SM}(k)$, *i.e.*,

$$v_1(k) = -B^{\dagger}\left[Ax_d(k) - x_d(k+1)\right]. \tag{5}$$

It is noted that Equation (5) is non-casual if the future desired output is unknown. In such a case, $x_d(k+1)$ could be estimated by the trapezoid estimation

$$x_d(k+1) = 2x_d(k) - x_d(k-1). \tag{6}$$

Substituting Equation (5) into Equation (4) yields

$$e(k+1) = Ae(k) + Bu_{SM} + D\varepsilon(k) + \left(I - BB^{\dagger}\right)Ax_d(k) - \left(I - BB^{\dagger}\right)x_d(k+1). \tag{7}$$

For the system described by Equation (3), one has $\left(I - BB^{\dagger}\right)Ax_d(k) - \left(I - BB^{\dagger}\right)x_d(k+1) = 0$. Thus, Equation (7) is simplified as

$$e(k+1) = Ae(k) + Bu_{SM} + D\varepsilon(k). \tag{8}$$

For the sliding function that takes the following form of

$$s(k) = Se(k). \tag{9}$$

The control action can be considered consisting two parts, *i.e.*,

$$u_{SM}(k) = u_{eq}(k) + \Delta u(k). \tag{10}$$

where $u_{eq}(k) = -(SB)^{-1}SAe(k)$ is the equivalent control and $\Delta u(k)$ is the switching control.

Substituting Equation (10) into Equations (8) and (9) yields

$$e(k+1) = \left[I - B(SB)^{-1}S\right]Ae(k) + B\Delta u(k) + D\varepsilon(k). \tag{11}$$

$$s(k+1) = SB\Delta u(k) + SD\varepsilon(k). \tag{12}$$

For the convenience of following discussion, Equations (9) and (11) are rewritten as

$$e(k+1) = A_e e(k) + B\Delta u(k) + D\varepsilon(k), \quad s(k) = Se(k). \tag{13}$$

where $A_e = \left[I - B(SB)^{-1}S\right]A$. The system described by Equation (13) can be equivalent as a dynamic plant, where $\Delta u(k)$ is the input and $s(k)$ is the output. The switching control is to force the plant output to be zero. For this, PID controller can be employed to generate the switching control such that the equivalent control error $s(k)$ is zero, which is given by

$$\Delta u(k) = -\left[Ps(k) + I\sum_{i=0}^{k} s(i)T + D\frac{s(k) - s(k-1)}{T}\right]. \tag{14}$$

where P, I and D are parameters of the discrete PID-based SMC; T is the sampling period.

Theorem 1: If the closed-loop system (13) is stable, the zero steady state error can be achieved [17].

Theorem 2: There exist some P, I and D such that the closed-loop control system (13) is stable [16].

3. Experiments

To verify the effectiveness of the proposed method, experiments were carried out to control the motion velocity of a stick-slip piezoelectric-driven actuator (**Figure 2**). The PEA used to drive the stage generates displacement in a range of 15 μm with a resolution of 0.5 nm. An inductive sensor (SMU9000, Kaman, Windsor, CT) with a resolution of 10 nm was used to measure the displacement of the end-effector. Both the actuator and the sensor were connected to a host computer via an I/O board (PCI-DAS1602/16, Measurement Computing Corporation) and controlled via SIMULINK programs. The movable stage is driven by the PEA and the end-effector on the stage can slide horizontally on the stage via a pair of V grooves machined on them. Polished silicon wafers are attached to the V grooves as frictional surfaces to guarantee the uniformity of the frictional characteristics throughout the traveling range of the end-effector. All the displacements presented in this study were measured by the inductive sensor with a sampling interval of 0.05 ms.

Figure 3 shows the model configuration of the stick-slip piezoelectric-driven stage developed in [18].

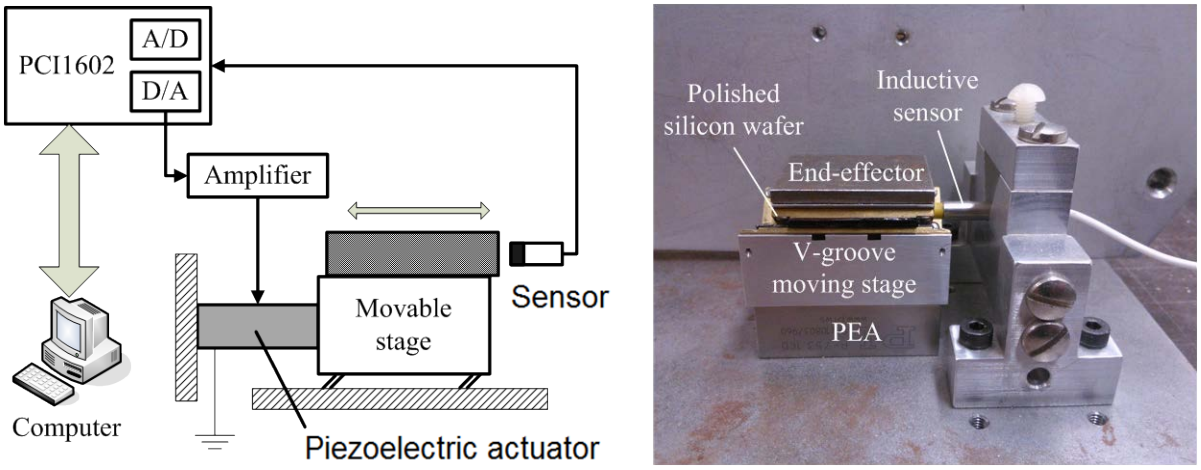

(a) (b)

Figure 2. Experimental settings on the piezoelectric driven stage; (a) schematic and (b) picture.

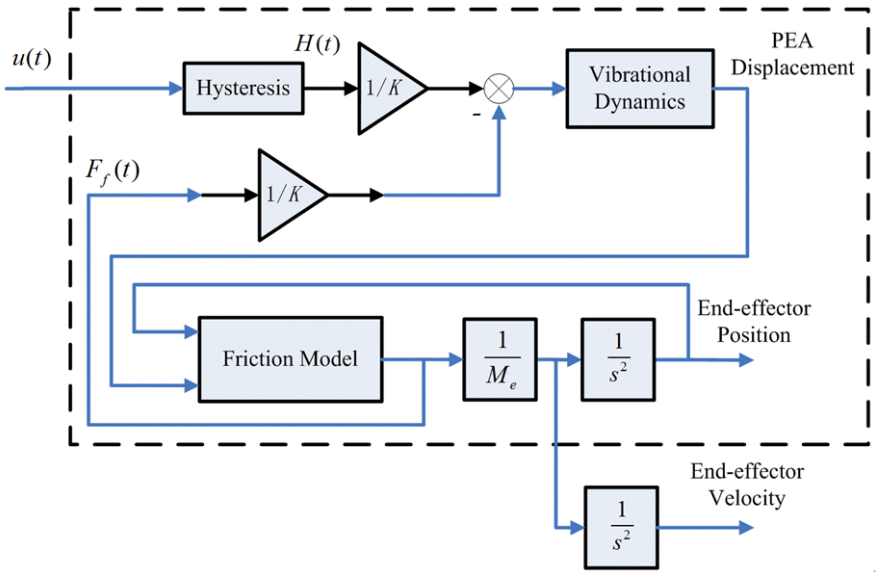

Figure 3. Model configuration of the piezoelectric-driven stick-slip actuator (Regenerated from [18]).

M_e is the mass of the end-effector, F_f is the friction force between the PEA stage and the end-effector. The hysteresis model H is cascaded with the vibration dynamics model. The output—PEA displacement is feed-forward to the friction model, which generates the friction force and the motion parameters of the end-effector.

To apply the ARX-based PID-SMC, the PEA and the end-effector are considered to be an integrated system with its input being the driven voltage u and its output being the motion velocity of the end-effector, as shown in **Figure 3**. The nonlinearities such as hysteresis and the friction are considered to be disturbances and then re-jected by the proposed method. Experiments for parameter identification were first carried out to obtain the ARX model. Then, the ARX-based PID-SMC was applied to control the nano-postioning stage for tracking step reference signals. Finally, dynamic tracking control with the proposed methods was implemented and compari-son to a PID controller was made.

3.1. Model Identification

To drive the end-effector, a saw-tooth generator is required, as seen in **Figure 4**. Each saw-tooth is 20 ms wide. The amplitude of the each saw-tooth is defined by the reference input voltage $u(t)$. If $u(t) < 0$, a reverse saw-

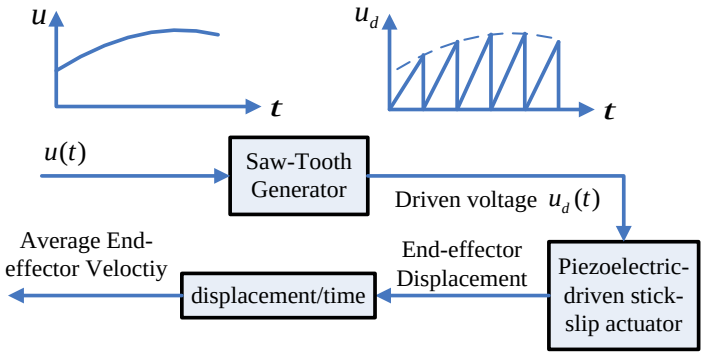

Figure 4. Saw-tooth generator for the stick-slip motion and the velocity calculator.

tooth signal is demanded to move the end-effector to the backward direction, as shown in **Figure 5**. The driven voltage supplied to the PEA u_d can be represented in terms of the reference input voltage as

$$\begin{aligned} &\text{if } u \geq 0,\ u_d(t) = u(t) \bmod (t,T)/T; \\ &\text{if } u < 0,\ u_d(t) = -u(t) + u(t) \bmod (t,T)/T. \end{aligned} \tag{15}$$

where T is the tooth width, mod represents the modulus after division.

The displacement of the end-effector is measured by the inductive sensor. The average velocity v is estimated by

$$v = \frac{S_{\text{saw-tooth}}}{T}. \tag{16}$$

where $S_{\text{saw-tooth}}$ is the displacement of the end-effector in one period of the saw-tooth signal.

The dynamics of the integral system can be regarded approximately as a second order system according to our previous research [19] [20]. As such, a second order ARX model was employed to describe the system dynamics, while the hysteresis exhibited by the actuator and the friction between the stage and the end-effector are considered as extra disturbances to the dynamic model. For the experiments, a 10 V step input reference voltage was provided to the PEA and the corresponding output velocity was estimated by Equation (23). With the recorded data, the parameters were identified by using the least square method, leading to

$$y(k) = 0.9985y(k-1) + 0.000972y(k-2) + 0.001458u(k-1). \tag{17}$$

3.2. Step Tracking

The ARX-based PID-SMC developed in this study was implemented in experiments to control the velocity of the piezoelectric-driven slick-slip actuator. The sliding surface was defined according to Equation (9), where $S = [m \quad 1]$ and $m = -0.1$. To minimize the rising time, the PID parameters in the PID regulator is adjusted to be $P = 0.2$, $I = 3$, $D = 0$. For comparison, the traditional PID controller was also applied, with its parameters adjusted by trails-and-errors to be $P = 0.4$, $I = 4$, $D = 0$.

Figure 6 shows the velocity step response of the piezoelectric-driven stick-slip actuator controlled by the developed control scheme and the traditional PID controller. **Table 1** shows the comparison of the rising time and the overshoot.

It can be seen that the tracking errors approach to zero through the use of I component in the PID regulator. The velocity step response of the piezoelectric-driven stick-slip actuator controlled by the proposed method is faster than that controlled by the traditional PID controller. For example, when a 10 μm/s step reference input was provided, the rising time of the velocity step response controlled by the ARX-based PID-SMC is 0.13 s, 0.2 ms less than that controlled by the PID controller. Faster velocity response is also observed for the 20 μm/s step reference input. However, since the dynamics performance of the piezoelectric-driven stick-slip actuator varies with the amplitude of the input voltage, the model error increased when the 20 μm/s step reference input was provided to the actuator. As a result, the overshoot increased to 10% in this case.

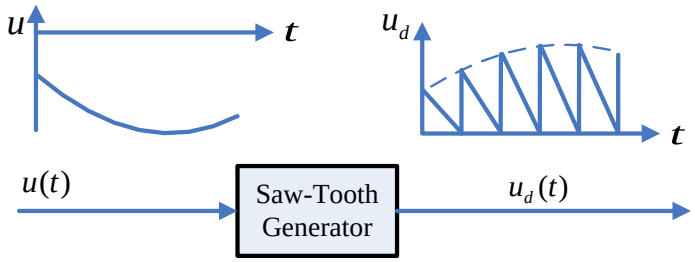

Figure 5. Reverse saw-tooth to driven the end-effector in the backward direction.

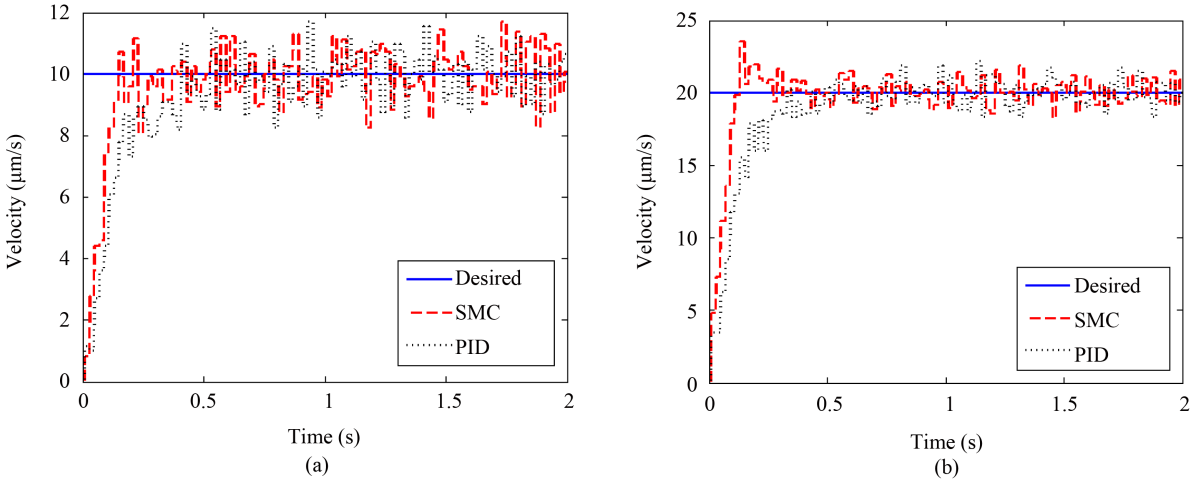

Figure 6. Velocity Step response of the piezoelectric-driven stick-slip actuator controlled by the proposed method and the traditional PID controller (a) 10 μm/s desired velocity; (b) 20 μm/s desired velocity.

Table 1. Comparison of the velocity step response between the ARX-based PID-SMC and the traditional PID controller.

Reference inputs	Controller	Rising time (s)	Overshoot (%)
10 μm/s step input	SMC	0.13	0
	PID	0.33	0
20 μm/s step input	SMC	0.11	10
	PID	0.21	0

To test the control performance of the proposed method, the same velocity step tracking experiments were also carried out with an increased mass of the end-effector. The same parameters is applied and compared with the traditional PID controller. **Figure 7** shows the velocity step response of the piezoelectric-driven stick-slip actuator controlled by the developed control scheme and the traditional PID controller. **Table 2** shows the comparison of the rising time and the overshoot. It can be concluded that the velocity step response of the piezoelectric-driven stick-slip actuator controlled by the proposed method is faster than that controlled by the traditional PID controller.

It is noted that the rising time of the velocity step response controlled by the ARX-based PID-SMC is 0.09 s. This is different from the result with an decreased mass of the end-effector, since the dynamics of the piezoelectric-driven stick-slip actuator also changes with the weight of the end-effector.

3.3. Sinusoidal Tracking

To further show the effectiveness of the proposed control method, sinusoidal tracking experiments with different

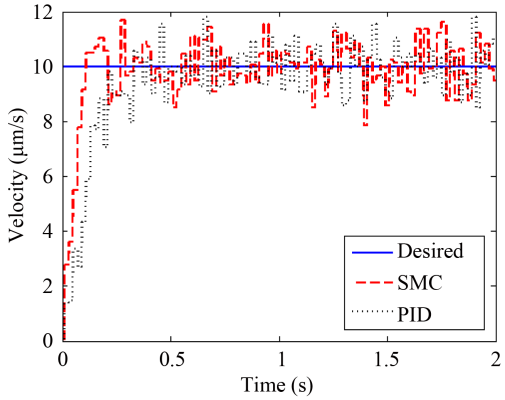

Figure 7. 10 μm/s Step response of the piezoelectric-driven stick-slip actuator controlled by the proposed method and the traditional PID controller.

Table 2. Comparison of the velocity step response between the ARX-based PID-SMC and the traditional PID controller with an increased mass of the end-effector.

Reference inputs	Controller	Rising time (s)	Overshoot (%)
10 μm/s step input	SMC	0.09	0
	PID	0.21	0

frequencies were carried out on the piezoelectric-driven stick-slip actuator. The same parameters were applied and the control performance was compared with the same PID controller. **Figure 8** shows the sinusoidal tracking performance of the piezoelectric-driven stick-slip actuator controlled by the proposed method and the traditional PID controller.

Table 3 compares the tracking error evaluated in terms of the 2-norm of the difference between the desired output and the measured output. From **Table 3**, it can be seen that the developed control scheme performs better than the traditional PID controller. As frequency increases, the priority of applying the ARX-based PID-SMC is more obvious. For example, for a 0.25 Hz 10 μm/s sinusoidal reference input, the tracking error with ARX-based PID-SMC is 1.12 μm, which is 29.7% of that with the PID controller. While for a 1 Hz sinusoidal reference input, the improvement increases to 40.2%.

It is noted that the velocity tracking performance deteriorates when the motion direction of the end-effector changes. For example, for 10 μm/s 1 Hz sinusoidal reference velocity, the maximum tracking error in time interval 0.5 - 0.75 s and 1.5 - 1.75 s is 50% of the amplitude if controlled by the ARX-based PID-SMC. The maximum tracking error even reaches 100% of the reference amplitude of the traditional PID controller is applied. This might be due to the nonlinear friction force between the end-effector and moving stage when the velocity changes from positive to negative. Obviously, the ARX-based PID-SMC partially compensates the nonlinearity. Consideration of the nonlinear friction model and its integration in the controller design are required for further improvement on the velocity tracking performance of the piezoelectric-driven stick-slip actuator.

4. Conclusion

This paper presents the development of an ARX-based PID-SMC for the velocity control of the piezoelectric-driven stick-slip actuator. Specifically, by applying ARX model, the output-tracking problem is defined as one of state tracking, while the “bang-bang” switching control in SMC is replaced with PID-based one. With the developed control scheme, chattering or the state oscillation at a high frequency can be eliminated and also the zero steady state error can be achieved. To verify the effectiveness of the developed control scheme, experiments were carried out on a piezoelectric-driven stick-slip actuator, whose dynamics was identified by experiments. The results of velocity tracking performance with the proposed control scheme were compared to that with the traditional PID controller. It was shown that both the step response and the sinusoidal tracking performance can be further improved by applying the proposed method, although the ARX model error exists. Howev-

Table 3. Comparison of the velocity step response between the ARX-based PID-SMC and the traditional PID controller with an increased mass of the end-effector.

Reference inputs	Frequency (Hz)	Tracking error (μm/s)	
		ARX-based PID-SMC	PID
10 μm/s sinusoidal input	0.25	1.12	1.57
	0.5	2.13	2.89
	1	2.82	4.72

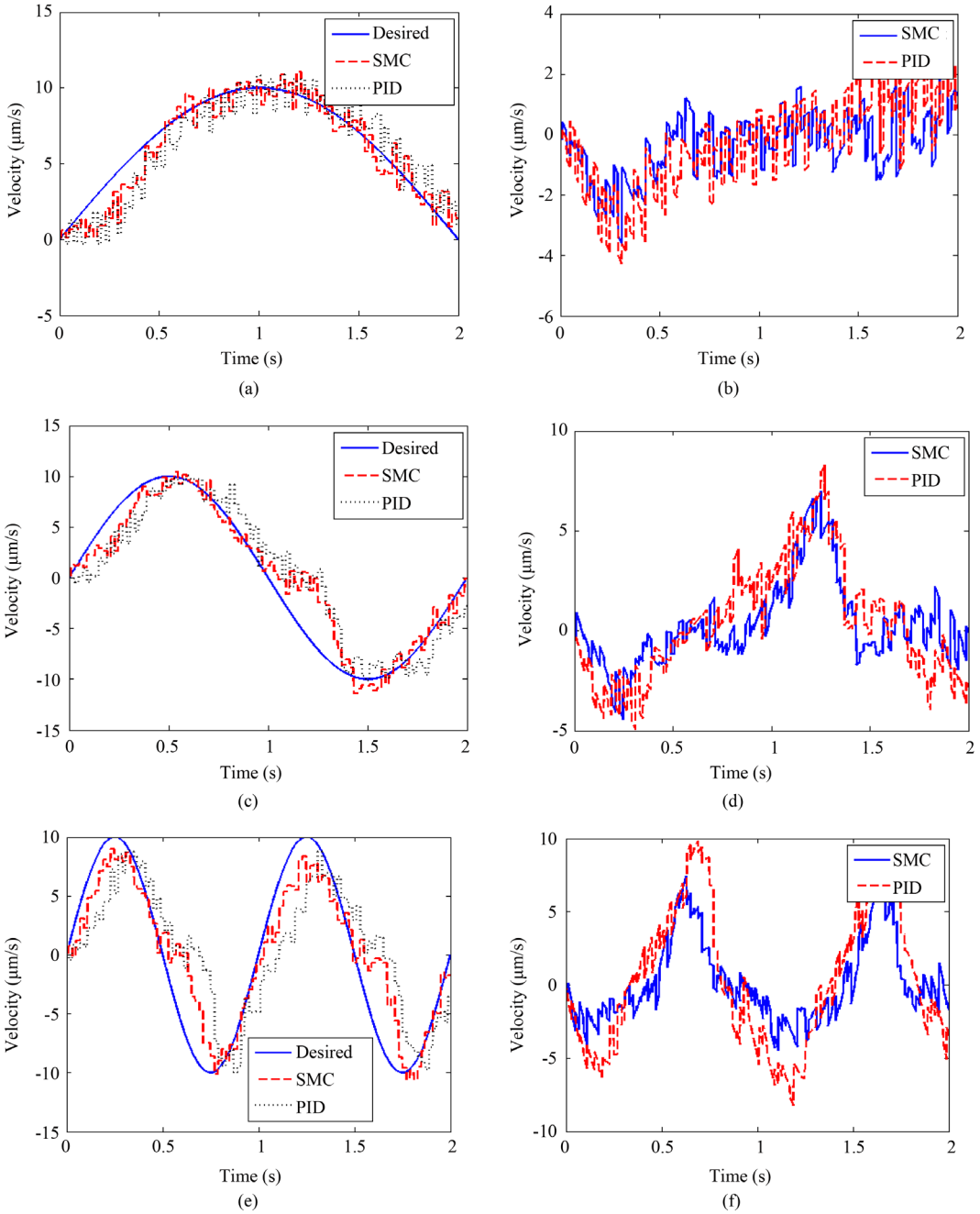

Figure 8. Comparison of sinusoidal tracking performance with different controllers: displacement and tracking error for (a) (b) 0.25 Hz frequency, (c) (d) 0.5 Hz frequency and (e) (f) 1 Hz frequency.

er, the control performance of the ARX-based PID-SMC depends on the accuracy of the identified dynamic model. This might be solved by employing a dynamic model with adaptive parameters and an adaptive ARX-based PID-SMC, which will be the focus of the future work. Furthermore, nonlinear friction model should be considered in the SMC design to further improve the velocity tracking performance of the piezoelectric-driven stick-slip actuator.

Acknowledgements

The support to the present study from the China Scholarship Council (CSC) and the Natural Sciences and Engineering Research Council (NSERC) of Canada is acknowledged.

References

[1] Devasia, S. and Moheimani, S.O.R. (2007) A Survey of Control Issues in Nano-Positioning. *IEEE Transactions on Control System Technology*, **15**, 802-823. http://dx.doi.org/10.1109/TCST.2007.903345

[2] Shiratori, H., Takizawa, M., Irie, Y., Hirata, S. and Aoyama, H. (2012) Development of the Miniature Hemispherical Tilt Stage Driven by Stick-Slip Motion Using Piezoelectric Actuators. *Mechatronics-REM*, Paris, 21-23 November.

[3] Zhang, Q.S., Chen, X.B. Yang, Q. and Zhang, W.J. (2012) Development and Characterization of a Novel Piezoelectric-Driven Stick-Slip Actuator with Anisotropic-Friction Surfaces. *International Journal of Advanced Manufacture Technology*, **61**, 1029-1034. http://dx.doi.org/10.1007/s00170-011-3771-y

[4] Eigoli, A.K. and Vossoughi, G. (2010) Dynamic Modeling of Stick-Slip Motion in a Legged Piezoelectric Driven Microrobot. *International Journal of Advanced Robotic Systems*, **7**, 201-208.

[5] Kang, D. (2012) Modeling of the Piezoelectric-Driven Stick-Slip Actuators. Master Thesis, College of Graduate Studies and Research, University of Saskatchewan, Saskatoon.

[6] Bergander, A. and Breguet, J.M. (1998) Performance Improvement for Stick-Slip Positioners. *International Symposium on Micromechatronics and Human Science*, 59-66.

[7] Spiller, M. and Hurak, Z. (2011) Hybrid Charge Control for Stick-Slip Piezoelectric Actuators. *Mechatronics*, **21**, 100-108. http://dx.doi.org/10.1016/j.mechatronics.2010.09.002

[8] Rakotondrabe, M., Haddab, Y. and Lutz, P. (2008) Voltage/Frequency Proportional Control of Stick-Slip Micropositioning Systems. *IEEE Transactions on Control System Technology*, **16**, 1316-1322. http://dx.doi.org/10.1109/TCST.2008.917232

[9] Rakotondrabe, M., Haddab, Y. and Lutz, P. (2009) Development of Modeling and Control of Mircro/Nano-Positioning 2-DOF Stick-Slip Device. *IEEE Transactions on Mechatronics*, **14**.

[10] Breguet, J.M. and Clavel, R. (1998) Stick and Slip Actuators: Design, Control, Performances and Applications. *International Symposium on Micromechatronics and Human Sciences*, Nagoya, 25-28 November 1998, 89-95.

[11] Young, K.D., Utkin, V.I. and Özgüner, Ü. (1999) A Control Engineer's Guide to Sliding Mode Control. *IEEE Transactions on Control System Technology*, **17**, 328-342. http://dx.doi.org/10.1109/87.761053

[12] Edwards, C. and Spurgeon, S.K. (1998) Sliding Mode Control. Taylor & Francis Ltd, London.

[13] Liawa, H.C., Shirinzadeh, B. and Smith, J. (2007) Enhanced Sliding Mode Motion Tracking Control of Piezoelectric Actuators. *Sensors and Actuators*, **A138**, 194-202. http://dx.doi.org/10.1016/j.sna.2007.04.062

[14] Wang, S., Habibi, S., Burton, R. and Sampson, E. (2006) Sliding Mode Control of an Electrohydraulic Actuator System with Discontinuous Nonlinear Friction. *Proceedings of the Institution of Mechanical Engineers*, **222**, Part I:J, Systems and Control Engineering.

[15] Peng, J.Y. and Chen, X.B. (2014) Integrated PID-Based Sliding Mode State Estimation and Control for Piezoelectric Actuators. *IEEE/ASME Transactions on Mechatronics*, **19**, 88-99. http://dx.doi.org/10.1109/TMECH.2012.2222428

[16] Cao, Y. and Chen, X.B. (2014) Disturbance Observer Based Sliding Mode Control for a Three-DOF Nano-Positioning Stage. *IEEE/ASME Transactions on Mechatronics*, **19**, 924-931. http://dx.doi.org/10.1109/TMECH.2013.2262802

[17] Cao, Y. and Chen, X.B. (2012) Integrated Inversion-Feedforward and PID-Based Sliding Mode Control for Piezoelectric Actuators. *American Control Conference*, Montreal, 27-29 June 2012.

[18] Peng, J.Y. and Chen, X.B. (2011) Modeling of Piezoelectric-Driven Stick-Slip Actuators. *IEEE/ASME Transactions on Mechatronics*, **16**, 394-399. http://dx.doi.org/10.1109/TMECH.2010.2043849

[19] Cao, Y. and Chen, X.B. (2012) A Novel Discrete ARMA-Based Model for Piezoelectric Actuator Hysteresis. *IEEE/ASME Transactions on Mechatronics*, **17**, 737-744. http://dx.doi.org/10.1109/TMECH.2011.2128339

[20] Chen, X.B., Zhang, Q.S., Kang, D. and Zhang, W.J. (2008) On the Dynamics of Piezoelectric Positioning Systems. *Review of Scientific Instrument*, **79**, Article ID: 116101. http://dx.doi.org/10.1063/1.2982238

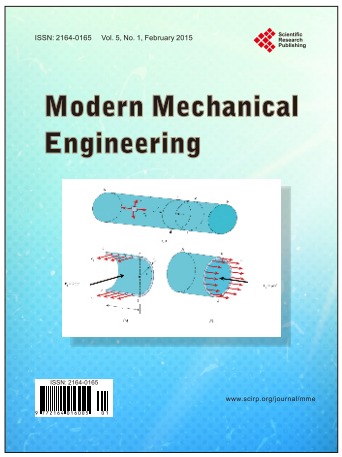

Call for Papers

Modern Mechanical Engineering

ISSN Print: 2164-0165 ISSN Online: 2164-0181
http://www.scirp.org/journal/mme

Modern Mechanical Engineering (MME) is an international journal dedicated to the latest advancement of mechanical engineering. The goal of this journal is to provide a platform for scientists and academicians all over the world to promote, share, and discuss various new issues and developments in different areas of mechanical engineering.

Editor in Chief

Editorial Board

Subject Coverage

All manuscripts must be prepared in English, and are subject to a rigorous and fair peer-review process. Accepted papers will immediately appear online followed by printed hard copy. The journal publishes original papers including but not limited to the following fields:

- Applied Mathematics and Mechanics
- Biomechanics
- Celestial Mechanics and Dynamical Astronomy
- Computational Mechanics
- Computer Methods in Applied Mechanics and Engineering
- Continuum Mechanics and Thermodynamics
- Damage Mechanics
- Engineering Fracture Mechanics
- Experimental Mechanics
- Mathematical Fluid Mechanics
- Mechanics in Medicine and Biology
- Mechanics of Composite Materials
- Mechanics of Materials
- Mechanism and Machine Theory
- Non-Linear Mechanics
- Non-Newtonian Fluid Mechanics
- Numerical and Analytical Methods in Geomechanics
- Rock Mechanics and Mining Sciences
- Solid and Structural Mechanics
- Theoretical and Applied Fracture Mechanics

We are also interested in: 1) Short Reports—2-5 page papers where an author can either present an idea with theoretical background but has not yet completed the research needed for a complete paper or preliminary data; 2) Book Reviews—Comments and critiques.

Website and E-Mail

http://www.scirp.org/journal/mme **E-mail: mme@scirp.org**

What is SCIRP?

Scientific Research Publishing (SCIRP) is one of the largest Open Access journal publishers. It is currently publishing more than 200 open access, online, peer-reviewed journals covering a wide range of academic disciplines. SCIRP serves the worldwide academic communities and contributes to the progress and application of science with its publication.

What is Open Access?

All original research papers published by SCIRP are made freely and permanently accessible online immediately upon publication. To be able to provide open access journals, SCIRP defrays operation costs from authors and subscription charges only for its printed version. Open access publishing allows an immediate, worldwide, barrier-free, open access to the full text of research papers, which is in the best interests of the scientific community.

- High visibility for maximum global exposure with open access publishing model
- Rigorous peer review of research papers
- Prompt faster publication with less cost
- Guaranteed targeted, multidisciplinary audience

Scientific Research Publishing

Website: http://www.scirp.org

Subscription: sub@scirp.org

Advertisement: service@scirp.org